OPTICS
AND LASER PHYSICS

Tomography of Optical Single-Qubit Quantum Memory

B. I. Bantysh[a, b]**, K. G. Katamadze**[a, b, *]**, Yu. I. Bogdanov**[a]**, K. I. Gerasimov**[c]**,**
M. M. Minnegaliev[c]**, R. V. Urmancheev**[c]**, and S. A. Moiseev**[c]

[a] *Valiev Institute of Physics and Technology, Russian Academy of Sciences, Moscow, 117218 Russia*
[b] *Quantum Technology Center, Faculty of Physics, Moscow State University, Moscow, 119991 Russia*
[c] *Kazan Quantum Center, Kazan National Research Technical University KAI, Kazan, 420111 Russia*
*e-mail: kgk@quantum.msu.ru
Received April 15, 2022; revised April 30, 2022; accepted May 15, 2022

Optical quantum memory is one of the basic elements of quantum information systems. However, the possibilities of its application in such systems sometimes can hardly be estimated by existing methods for its characterization. In this work, the tomography of quantum memory has been implemented as a *quantum process in a logical basis*. It has been shown that the implemented quantum memory scheme for polarization photon qubits with a high accuracy corresponds to the identity transformation and is promising for application in quantum communication and quantum computing.

1. INTRODUCTION

The development of efficient optical quantum memory (QM) is important for quantum information technologies. One of the basic aims relevant for optical quantum communications and quantum computing technologies is the storage of polarization qubits in optical QM [1, 2]. Crystals with rare-earth ions open wide possibilities for implementing optical QM because of a long lifetime of optical and spin coherences of quantum transitions [3, 4]. Such crystals usually provide anisotropic absorption of light radiation with different polarizations [5], which complicates the storage of quantum states of polarization qubits in them. At least two methods for implementing such QM are known. In the first method, orthogonal (horizontal, H, and vertical, V) polarization components of radiation are stored in different spatial modes of the same crystal and are then joined in a single spatial mode of the restored signal [6]. In the second method, two crystals are used to store polarization states of the signal [7, 8]. One of the signal polarization components is rotated by 90° and is stored in a crystal with the same parameters of optical QM. The experiments reported in [6−8] show a sufficiently high accuracy of storage of polarization qubits. However, experimental difficulties of using various spatial modes or several crystals make it possible to search for easier ways to implement optical QM for polarization qubits.

In this work, we implement optical QM for polarization qubits in a single spatial mode of the Tm^{3+}:$Y_3Al_5O_{12}$ ($c = 0.1$ at %) crystal, which has different efficiencies of recovery for orthogonal polarization components of the photonic qubit. To characterize QM under study, we develop the quantum tomography technique based on a *quantum process in a logical basis* [9, 10]. Quantum tomography can reconstruct with a high accuracy the parameters of quantum transformations performed by devices and then correct the operation of these devices and the choice of their parameters to ensure the necessary accuracy of quantum operations. We perform the quantum tomography of storage of polarization qubits in optical QM based on the photon echo effect [11, 12] on an optical transition of thulium ions in the Tm^{3+}:$Y_3Al_5O_{12}$ ($c = 0.1$ at %) crystal with an inhomogeneous broadening in the form of an atomic frequency comb [13].

The tomography procedure is based on the adequacy and accuracy criteria and the root approach to the parameterization of the χ matrix, which makes it possible to vary the rank of a quantum process [9, 10, 14, 15]. Furthermore, in order to separate the error of the quantum process and the error of preparation and measurement of quantum states, we first carried out the tomography of the identity transformation and took into account its results when reconstructing the optical QM process. We showed that the resulting quantum process matrix coincides with an accuracy up to 96% with the ideal identity transformation.

To determine the source of errors, we developed a model of the quantum process in the single-qubit basis taking into account different quantum efficiencies for different polarization modes and background noise. It was shown that the developed model adequately describes the results and its application demonstrates that the quantum state of the polarization qubit can be
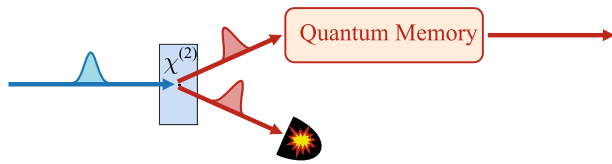
Fig. 1. (Color online) Application of optical quantum memory to fabricate a demanded single-photon source.

restored with a high accuracy in the proposed optical QM scheme.

2. OPTICAL QUANTUM MEMORY AND APPROACHES TO ESTIMATE ITS QUALITY

One of the important applications of optical quantum memory is the development of efficient demanded single-photon sources based on heralded conditional sources [2] (Fig. 1). Heralded single-photon sources are based on processes where a pair of photons are created with a certain probability in two correlated optical modes in a nonlinear optical process (spontaneous parametric down conversion or spontaneous four-wave mixing) induced by a pump laser pulse. Then, the detection of a photon in one of the channels indicates with a high probability the presence of the second photon in the conjugate channel. Such a conditional probability of triggering heralded single-photon sources currently reaches 97% [16], which is much higher than that for demanded single-photon sources (60% [17]). The introduction of QM in the considered technology will make it possible to store a photon at the time of triggering the detector and then to emit it at a given different time. Thus, quantum memory can solve the problem of the efficient synchronization of demanded single-photon sources.

Losses in the optical channel leading to errors are crucial for optical communication. Quantum repeaters can solve this problem [18]. They are chains of sequentially connected sources of entangled photons and detectors ensuring measurements in the basis of Bell states (Fig. 2). Then, if all detectors are triggers, photons on the opposite ends of a chain are in an entangled state and can be used, e.g., for key distribution according to the Ekert protocol. However, the implementation of such a chain is problematic because sources of entangled photon pairs usually operate in the spontaneous mode; i.e., they are triggered only with a certain very low probability. Such sources can also be synchronized using QM. In this application, this memory should not only store a photon but also store its polarization or phase state, which is used to encode quantum information.

One of the most promising physical platforms for quantum computing is a photon platform. Its evident advantage is the possibility of avoiding decoherence. However, the absence of the interaction between photons is its demerit. Nevertheless, this platform has already demonstrated quantum advantage [19], and the one-way quantum computing architecture is promising for implementing practically important quantum algorithms. Within this approach, a high-dimensional entangled (cluster) state is first prepared and the entire subsequent algorithm is reduced to the sequential measurement and unitary transformation of individual qubits. The type of each unitary transformation depends on the results of measurements of all preceding qubits. Entangled optical states (even low-dimensional) are usually obtained probabilistically; consequently, numerous sources of low-dimensional entangled state should be synchronized to prepare cluster states. Then, the measurement and transformation of individual qubits should be synchronized to implement computing. All these procedures also require QM, which should in this case allow storing not only individual qubits but also cluster states with
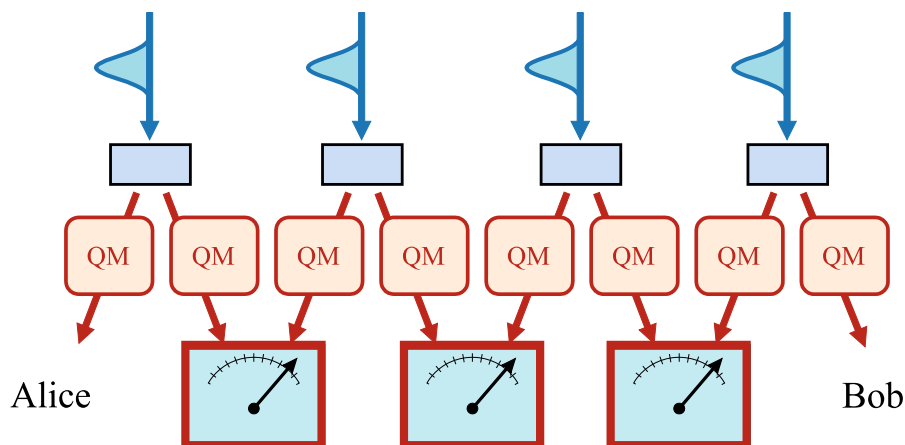

Fig. 2. (Color online) Application of quantum memory in quantum repeaters.
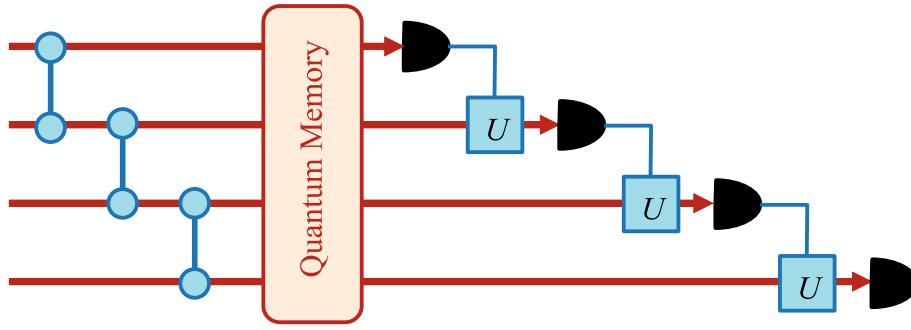
Fig. 3. (Color online) Application of quantum memory in the one-way quantum computer architecture.

the possibility of sequential addressed extraction of qubits one-by-one (Fig. 3).

Thus, to understand the possibilities of application of optical QM in quantum information systems, it is necessary to study its properties as a single- or multiqubit process. However, the corresponding studies are usually reduced only to the determination of low-level technical characteristics such as the lifetime/storage time, efficiency, and presence of noise. The authors of [20, 21] performed tomography of QM as a single-mode quantum process in the infinite basis of quadrature or Fock states of light. This approach makes it possible to reveal imperfections in the implementation of QM, but its generalization even to the two-mode case corresponding to single-qubit QM crucially increases the dimension of the problem, making it hardly solvable both in the number of measurements and in computing difficulty. At the same time, in practice, it is not necessary to consider infinite-dimensional multimode Fock spaces; it is sufficient to consider a subspace corresponding to the logical values of qubits. This problem is much simpler and will allow in future the characterization of multiqubit QM.

3. EXPERIMENTAL IMPLEMENTATION OF THE QUANTUM MEMORY PROTOCOL BASED ON ATOMIC FREQUENCY COMBS

The experimental sample was optical QM based on the photon echo in a $Tm^{3+}:Y_3Al_5O_{12}$ crystal with an impurity ion concentration of 0.1 at %, where an atomic frequency comb with 11 peaks spaced by $\Delta = 2.5$ MHz was created on the 793.37-nm $^3H_6(1)-$ $^3H_4(1)$ optical transition. The crystal was placed in a weak external magnetic field $\mathbf{B} \parallel [001]$ at a temperature of 3.4 K. The process of initialization was similar to those described in [13, 22, 23]. Stored optical pulses had a Gaussian time profile with a FWHM duration of $\delta t_s = 150$ ns. A disadvantage of this protocol is the preset storage time $t_{echo} = \tau = 400$ ns, and its advantage is the absence of optical noise because the time interval from the initialization (or production) of the atomic

frequency comb to the emission of the stored pulse is much longer than the lifetime of the excited optical state and spontaneous emission from the excited state is insignificant. At the same time, it is known that, using the Stark (Zeeman) effect in rare-earth ions in external electric (magnetic) fields, one can controllably dephase and rephase excited optical and spin coherence [24, 25]. Thus, the emission time of the photon echo signal can be multiplied as $t_{echo} = n\tau$ ($n = 1, 2, ...$) and demanded reading of the input signal can be implemented [26, 27].

Polarization degrees of freedom were used to encode information. The $|0\rangle$ and $|1\rangle$ logical states corresponded to the state of one photon in horizontally and vertically polarized modes, respectively. A demerit of such encoding to implement optical quantum memory is that the quantum efficiencies are different: $\eta_H = 13.8\%$ and $\eta_V = 7\%$ for the horizontal and vertical polarizations, respectively.

The layout of the experimental setup for the tomography of optical quantum memory is shown in Fig. 4. Input states are prepared by means of laser pulses attenuated by an attenuator (Att). Their polarization is fixed by a polaroid (P) and is then transformed by half-wave (HWP1) and quarter-wave (QWP1) phase plates. Thus, an arbitrary polarization state of light can be stored in QM. Optical pulses extracted from memory are reflected by a mirror (M), pass through half-wave (HWP2) and quarter-wave (QWP2) phase plates, and are then split by a polarization beam splitter PBS into two channels, where detectors D1 and D2 are placed. Measurements are carried out in both the multiphoton and quasi-single-photon regimes. In the multiphoton regime, the attenuation factor of the attenuator is chosen such that the average number of photons in a pulse is much larger than one, and linear photodetectors are used to record such pulses. In the quasi-single-photon regime, pulses are attenuated to the average number of photons $\mu = 0.88$ and are detected by silicon avalanche photodiodes operating in the photon count mode. The echo count histogram based on atomic frequency combs for
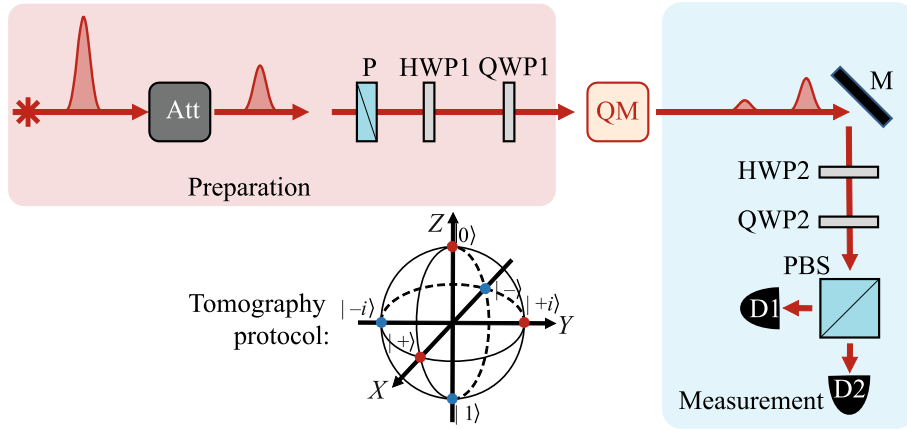
Fig. 4. (Color online) Layout of the experimental setup for the tomography of single-qubit quantum memory and the quantum process tomography protocol.

storing and restoring the $|1\rangle$ state at a time of 0.4 μs is exemplified in Fig. 5.

4. RECONSTRUCTION OF THE QUANTUM MEMORY PROCESS

The general single-qubit quantum process can be defined in terms of the χ matrix, which ensures the following transformation of the density matrix:

$$\rho_{out} = \sum_{\alpha,\beta} \chi_{\alpha\beta} A_\alpha \rho_{in} A_\beta^\dagger, \quad \alpha,\beta = I, X, Y, Z, \quad (1)$$

where

$$A_I = \frac{\sigma_0}{\sqrt{2}}, \quad A_X = \frac{\sigma_x}{\sqrt{2}}, \quad A_Y = \frac{\sigma_y}{\sqrt{2}}, \quad A_Z = \frac{\sigma_z}{\sqrt{2}}$$
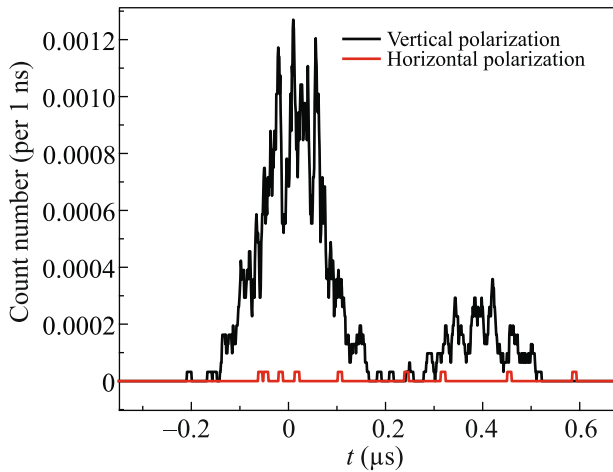

Fig. 5. (Color online) Example of the echo count histogram based on atomic frequency combs for storing and restoring the $|1\rangle$ state at a time of 0.4 μs.

constitute the normalized basis of Pauli matrices. The 4×4 χ matrix with the elements $\chi_{\alpha\beta}$ has a trace of 2 and can be represented in the form $\chi = ee^\dagger$, where e is the $4 \times r$ matrix and $r = 1, 2, 3,$ or 4 is the rank of the quantum operation. Varying the rank, one can obtain the maximum accuracy of the reconstruction of the process parameters, thus ensuring the adequacy of the model to experimental data.

For the full tomography of a quantum process, it is necessary to feed some set of states to the entrance and to conduct mutually supplementary measurements of the input states. In this work, we choose the "cube protocol" with six input states $|b_j\rangle = \{|+\rangle, |-\rangle, |+i\rangle, |-i\rangle, |0\rangle, |1\rangle\}$, where the projectors $P_i = |b_i\rangle\langle b_i|$ corresponding to the observables X, Y, and Z are measured at the output. These states and observables are indicated on the Bloch sphere in the inset of Fig. 4.

At the first stage, the measurement scheme was calibrated in the absence of QM in the multiphoton regime; i.e., the tomography of the identity transformation was carried out. It was found that the mirror (M) in the measurement scheme introduces an additional phase difference between horizontally and vertically polarized radiation, which is described by an additional unitary transformation of polarization qubits with the matrix $U_M = \begin{pmatrix} 0.36 + 0.93i & -0.08 - 0.03i \\ 0.08 - 0.03i & 0.36 - 093i \end{pmatrix}$, which approximately corresponds to the rotation of the qubit on the Bloch sphere about the Z axis [28] by an angle of $-137°$. The measurement protocol was correspondingly corrected, and the measurements are described by the projectors $P'_j = U_M^\dagger P_j U_M$.

The second stage of tomography was conducted in the quasi-single-photon mode. To reconstruct the parameters of QM, we used a rank-1 model that does not conserve the trace of the process because this
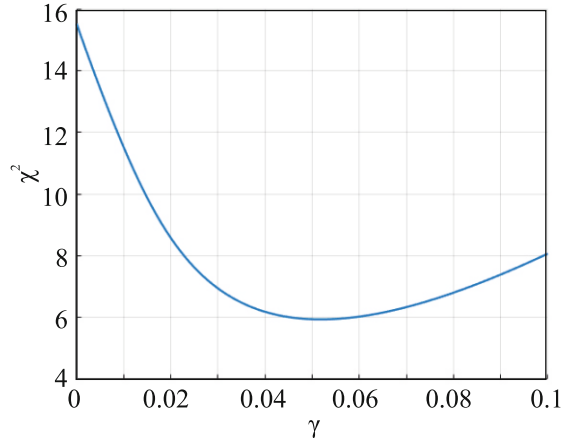
Fig. 6. (Color online) Quantity χ^2 versus the noise parameter γ in the measurement model.

memory is characterized by asymmetric efficiencies for the horizontal and vertical polarization components. Dark noise of detectors plays a significant role in the quasi-single-photon measurement. The standard approach involves the simple subtraction of such noise from statistical data. A more correct approach requires the modification of the measurement model itself. This modification corresponds to the correction of the measurement operators as $P_j'' = \dfrac{P_j' + \gamma I}{2\gamma + 1}$, where γ is the noise coefficient. To choose the optimal γ value, we minimized the quantity $\chi^2 = \sum_{j=1}^{m} (O_j - E_j)^2 / E_j$, where O_j and E_j are the detected and expected numbers of counts, respectively. Figure 6 shows their dependence on the considered noise parameter. The minimum of this func-

tion is ensured at the value $\gamma = 0.052$, corresponding to the calculated value $\gamma = \dfrac{2d}{\langle \eta \rangle \mu} = 0.050$, where $d = \tau R = 0.0023$ is the probability of dark triggering of the detector during the pulse readout time. Therefore, the used QM protocol based on the atomic frequency comb indeed does not introduce additional optical noise. The value $\gamma = 0.052$ is used below to develop an adequate model of the quantum process.

The reconstruction of the rank-1 process yields the nonunitary matrix

$$J = \begin{pmatrix} 0.8234 - 0.0091i & -0.0564 - 0.0824i \\ -0.0149 - 0.0783i & 1.1426 + 0.0127i \end{pmatrix}, \quad (2)$$

which can be interpreted as the Jones matrix of the process executed by quantum memory. This matrix is defined with accuracy to the general losses of the entire measurement scheme. Its normalization $\text{Tr}(J^\dagger J) = 2$ coincides with the normalization of an arbitrary unitary matrix, in particular, the identity matrix. This allows one to analyze the capability of QM to store the logical states of a polarization qubit. The χ matrix of the transformation given by Eq. (2) is shown in Fig. 7.

The Pauli transfer matrix of this process has the form

$$R = \begin{pmatrix} 1 & -0.0636 & -0.0209 & -0.3156 \\ -0.0770 & 0.9480 & -0.0177 & 0.0539 \\ 0.0288 & 0.0240 & 0.9334 & -0.1580 \\ -0.3120 & -0.0277 & 0.1576 & 0.9837 \end{pmatrix}.$$

It is equivalent to the Müller matrix of the polarization transformation. The first row of this matrix describes the degree of conservation of the trace of the process. For processes conserving the trace, the first row has
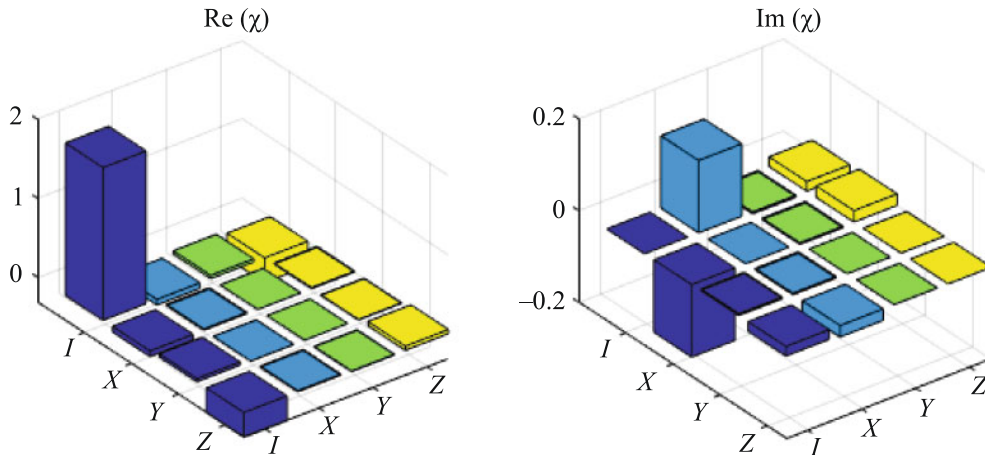

Re (χ) Im (χ)

Fig. 7. (Color online) χ matrix of the restored quantum memory process in the Pauli representation. For an ideal identity transformation, all elements of the χ matrix are zero except for $\chi_{II} = 2$ (in this case, Eq. (1) ensures the identity transformation).
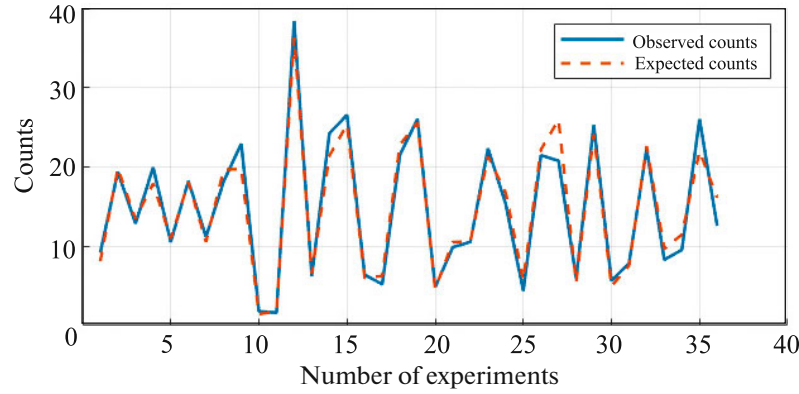
Fig. 8. (Color online) Theoretical (based on the restored rank-1 process) and experimental numbers of photocounts in each of the 36 measurements of the quantum process tomography protocol.

the form (1000). The first column of the matrix R characterizes the degree of unitality of the process. For unital processes, the first column has the form $(1000)^T$. The matrix R for the ideal identity process is the identity matrix.

The accuracy of the resulting transformation relative to the identity process is 96.63%. Figure 8 shows theoretical and experimental numbers of photocounts. The Pearson correlation coefficient between these two sets is 0.9806. Good agreement between experimental data and the developed theoretical model clearly demonstrated in Fig. 7 is also confirmed by the χ^2 criterion.

Within a more complex rank-2 model, the reconstructed χ matrix has eigenvalues of 1.9733 and 0.0267. The Kraus operators have the form

$$E_1 = \begin{pmatrix} -0.8201 & 0.0572 + 0.0819i \\ 0.0157 + 0.0769i & -1.1331 - 0.0248i \end{pmatrix},$$

$$E_2 = \begin{pmatrix} -0.1117 & -0.0363 - 0.0209i \\ -0.0813 - 0.0039i & 0.0759 + 0.0087i \end{pmatrix}.$$

The contribution from the second component is as small as about 1.3%.

5. CONCLUSIONS

The review of areas of application of optical quantum memory and approaches to its characterization have shown that the existing methods of characterizing optical quantum memory cannot completely estimate the possibility of its application in quantum information. To obtain the most adequate estimate, it is necessary to consider quantum memory as a quantum process in the logical basis of qubits. Within this approach, we have performed the experimental tomography of optical quantum memory based on the photon echo effect in the $Tm^{3+}:Y_3Al_5O_{12}$ crystal. The polarization degrees of freedom of photons with dif-

ferent restoring efficiencies for the orthogonal polarization components of a photon qubit have been used to encode qubits. At the first stage, we have performed the calibration of the experimental setup corresponding to the tomography of the identity transformation in the multiphoton mode. It has been found that the measurement scheme involves an additional unitary transformation, which has been taken into account in subsequent experiments. The tomography of single-qubit quantum memory in the quasi-single-photon mode has been performed at the second stage. To develop an adequate measurement model, we have taken into account dark noise of single-photon detectors. As a result, it has been shown that a rank-1 process can be used to describe single-qubit quantum memory. Such a model adequately reproduces experimental data with a correlation coefficient of 0.9806. The matrix of the resulting process corresponds to the identity transformation with an accuracy of 96.63%, which indicates that implemented optical quantum memory can be applied in quantum information problems. To summarize, the quantum memory tomography procedure as a single-qubit quantum process has been developed and successfully approved in the experiment. It has been shown that the relation between the amplitude and phase difference between quasi-single-photon states does not significantly change. In the future, the developed method can be generalized to the multiqubit case, which will allow, in particular, the analysis of the accuracy of conservation of the entanglement of quantum states. We note that the efficiency of quantum memory, as well as the accuracy of restoring the signal pulse, can be increased by placing the working medium in a cavity with optimal parameters [25]. The use of a system of several interacting cavities is also possible [29, 30], which opens new possibilities of implementing quantum memory and of expanding its working spectral range.

CONFLICT OF INTEREST

The authors declare that they have no conflicts of interest.

REFERENCES

1. N. Sangouard, C. Simon, H. de Riedmatten, and N. Gisin, Rev. Mod. Phys. **83**, 33 (2011).

2. K. Heshami, D. G. England, P. C. Humphreys, P. J. Bustard, V. M. Acosta, J. Nunn, and B. J. Sussman, J. Mod. Opt. **63**, 2005 (2016).

3. P. Goldner, A. Ferrier, and O. Guillot-Noël, *Rare Earth-Doped Crystals for Quantum Information Processing, Handbook on the Physics and Chemistry of Rare Earths* (Elsevier, Amsterdam, 2015).

4. M. Zhong, M. P. Hedges, R. L. Ahlefeldt, J. G. Bartholomew, S. E. Beavan, S. M. Wittig, J. J. Longdell, and M. J. Sellars, Nature (London, U.K.) **517**, 177 (2015).

5. S. R. Hastings-Simon, M. Afzelius, J. Minář, M. U. Staudt, B. Lauritzen, H. de Riedmatten, N. Gisin, A. Amari, A. Walther, S. Kröll, E. Cavalli, and M. Bettinelli, Phys. Rev. B **77**, 125111 (2008).

6. M. Gündoğan, P. M. Ledingham, A. Almasi, M. Cristiani, and H. de Riedmatten, Phys. Rev. Lett. **108**, 190504 (2012).

7. C. Clausen, F. Bussiéres, M. Afzelius, and N. Gisin, Phys. Rev. Lett. **108**, 190503 (2012).

8. Z.-Q. Zhou, W.-B. Lin, M. Yang, C.-F. Li, and G.-C. Guo, Phys. Rev. Lett. **108**, 190505 (2012).

9. Y. I. Bogdanov, A. A. Kalinkin, S. P. Kulik, E. V. Moreva, and V. A. Shershulin, New J. Phys. **15**, 035012 (2013).

10. Yu. I. Bogdanov, B. I. Bantysh, A. A. Kalinkin, S. P. Kulik, E. V. Moreva, and V. A. Shershulin, J. Exp. Theor. Phys. **118**, 845 (2014).

11. S. A. Moiseev and B. S. Ham, Phys. Rev. A **70**, 063809 (2004).

12. W. Tittel, M. Afzelius, T. Chaneliére, R. L. Cone, S. Kröll, S. A. Moiseev, and M. Sellars, Laser Photon. Rev. **4**, 244 (2009).

13. T. Chaneliere, J. Ruggiero, M. Bonarota, M. Afzelius, and J.-L. Le Gouët, New J. Phys. **12**, 023025 (2010).

14. Y. I. Bogdanov, G. Brida, I. D. Bukeev, M. Genovese, K. S. Kravtsov, S. P. Kulik, E. V. Moreva, A. A. Soloviev, and A. P. Shurupov, Phys. Rev. A **84**, 042108 (2011).

15. B. I. Bantysh, A. Yu. Chernyavskiy, and Yu. I. Bogdanov, JETP Lett. **111**, 512 (2020).

16. P. Ben Dixon, D. Rosenberg, V. Stelmakh, M. E. Grein, R. S. Bennink, E. A. Dauler, A. J. Kerman, R. J. Molnar, and F. N. C. Wong, Phys. Rev. A **90**, 043804 (2014).

17. H. Wang, Y. M. He, T. H. Chung, et al., Nat. Photon. **13**, 770 (2019).

18. H. J. Briegel, W. Dür, J. I. Cirac, and P. Zoller, Phys. Rev. Lett. **81**, 5932 (1998).

19. H.-S. Zhong, H. Wang, Y.-H. Deng, et al., Science (Washington, DC, U. S.) **370**, 1460 (2020).

20. M. Hosseini, G. Campbell, B. M. Sparkes, P. K. Lam, and B. C. Buchler, Nat. Phys. **7**, 794 (2011).

21. M. Lobino, C. Kupchak, E. Figueroa, and A. I. Lvovsky, Phys. Rev. Lett. **102**, 1 (2009).

22. M. Bonarota, J. Ruggiero, J. L. L. Gouët, and T. Chaneliére, Phys. Rev. A **81**, 1 (2010).

23. M. Bonarota, J. L. le Gouët, S. A. Moiseev, and T. Chaneliere, J. Phys. B: At. Mol. Opt. Phys. **45**, 124002 (2012).

24. K. I. Gerasimov, S. A. Moiseev, and R. B. Zaripov, Appl. Magn. Reson. **48**, 795 (2017).

25. M. M. Minnegaliev, K. I. Gerasimov, R. V. Urmancheev, A. M. Zheltikov, and S. A. Moiseev, Phys. Rev. B **103**, 174110 (2021).

26. S. P. Horvath, M. K. Alqedra, A. Kinos, A. Walther, J. M. Dahlström, S. Kröll, and L. Rippe, Phys. Rev. Res. **3**, 023099 (2021).

27. I. Craiciu, M. Lei, J. Rochman, J. G. Bartholomew, and A. Faraon, Optica **8**, 114 (2021).

28. M. A. Nielsen and I. L. Chuang, *Quantum Computation and Quantum Information* (Cambridge Univ. Press, Cambridge, 2000).

29. S. A. Moiseev and N. S. Perminov, JETP Lett. **111**, 500 (2020).

30. S. A. Moiseev, N. C. Perminov, and A. M. Zheltikov, JETP Lett. **115**, 318 (2022).

Translated by R. Tyapaev